2002

Simulating Shape Changes during Electrodeposition: Primary and Secondary Current Distribution

Venkat R. Subramanian
University of South Carolina - Columbia

Ralph E. White
University of South Carolina - Columbia, white@cec.sc.edu

Publication Info

Published in *Journal of the Electrochemical Society*, Volume 149, Issue 10, 2002, pages C498-C505.

Subramanian, V.R., & White, R.E. (2000). Simulating Shape Changes during Electrodeposition: Primary and Secondary Current Distribution. *Journal of the Electrochemical Society*, *149*(10): C498-C505.
Publisher's Version: http://dx.doi.org/10.1149/1.1505637

Journal of The Electrochemical Society, **149** (10) C498-C505 (2002)
0013-4651/2002/149(10)/C498/8/$7.00 © The Electrochemical Society, Inc.

Simulating Shape Changes during Electrodeposition

Primary and Secondary Current Distribution

Venkat R. Subramanian*,z and Ralph E. White**

Department of Chemical Engineering, University of South Carolina, Columbia, South Carolina 29208, USA

A technique based on the analytical method of lines is presented for predicting shape changes during electrodeposition. The technique is presented for both primary and secondary current distributions. The method presented does not require iterations for nonlinear Butler-Volmer boundary conditions or changing electrode shapes. The technique is based on a semianalytical method developed earlier for predicting current distributions in electrochemical cells. This technique is attractive because it provides a symbolic solution for the Laplace equation, and hence requires less computation time to perform case studies.
 [DOI: 10.1149/1.1505637]

Manuscript submitted December 3, 2001; revised manuscript received March 28, 2002. Available electronically September 10, 2002.

Potential distributions and their associated current density distributions (primary and secondary) are typically obtained by solving Laplace's equation.[1-3] The methods used to solve Laplace's equation include analytical and numerical methods. Analytical methods (*e.g.*, conformal mapping[4]) provide the maximum insight into the problem and usually yield closed form potential and current distributions. Unfortunately, analytical techniques are system specific, are restricted to linear kinetics, and are often difficult to obtain. Numerical techniques are very general, but usually give a numerical value for the potential at a particular location. A new technique (semianalytical method or analytic method of lines) was developed[5] and shown to be more general than a particular analytical solution technique; it gave better insight than numerical techniques for a certain class of problems (Laplace equation which has constant coefficients in at least one of the independent variables). Note that the semianalytical method presented earlier[5] for solving Laplace's equation in two spatial coordinates with nonlinear boundary conditions does not require iterations for interior node points as is the case for numerical methods.[6] Nonlinearities of the boundary conditions can be removed by solving for the constants that appear in the solution of Laplace's equation using our analytic method of lines.[5]

During electrodeposition of a metal (*e.g.*, copper) on a substrate, the deposit grows on the cathode. Since the shape of the cathode changes during deposition, the potential and current distributions are usually solved numerically.[7-11] Numerical methods reported in the literature[7-11] for solving the Laplace equation include finite difference, finite element, and boundary element techniques. Georgiadou *et al.*[11] developed an adaptive finite element method for simulating shape changes. Numerical methods reported in the literature require solving the Laplace equation for every time step because the shape of the cathode changes, and the numerical methods require solving the Laplace equation again for a new geometry. In addition, for every time step the existing numerical methods in the literature requires iterations until convergence for solving the Laplace equation with nonlinear Butler-Volmer boundary conditions. Our semianalytical method provides a means for solving for the Laplace equation with nonlinear Butler-Volmer boundary conditions without iterations. Another advantage of the semianalytical method is that the method is valid for arbitrary cathode shapes as shown for a sinusoidal electrode.[5] The flexibility of the semianalytical method in handling nonlinear boundary conditions and arbitrary electrode shapes is exploited in this investigation to predict the shape changes during electrodeposition. Another unique aspect of the semianalytical technique is that the method yields both potential and current distributions simultaneously. This avoids numerical inaccuracies that result from numerical differentiation of the potential distribution to find the current distribution.

Recently, West *et al.*[12] and Gill *et al.*[13] presented models for predicting copper electrodeposition in vias and trenches.[12,13] In their models, they assumed that the deposit grows in one dimension. In this paper, we present a technique for modeling the deposit growth in one dimension (1-D) where the potential is governed by the Laplace equation in 2-D.

Theoretical Formulation

The 2-D cell to be modeled is shown in Fig. 1. The cathode is of primary interest and is at the bottom of the cell and the anode is coplanar with the upper insulating plane. The sidewalls represent either insulating surfaces or planes of symmetry. Between the electrodes is an electrolytic solution of uniform composition. Electrodeposition of metal at the cathode occurs at constant cell voltage. This geometry is chosen as it restricts the growth to 1-D. The technique developed is general and can handle geometries with singularities (*e.g.*, at the anode/insulator interface ($x = l/2$; $y = b$) where the current density is infinite).

The following assumptions are made: (*i*) A single cathodic reaction takes place at the cathode. (*ii*) The anode is unpolarized and does not change shape during electrolysis. (*iii*) The transport and kinetic parameters do not vary in space or time. (*iv*) The shape change is restricted to 1-D (y).

Primary current distribution.—The governing equation for the potential field in the electrolytic solution obeys the Laplace equation[1]

$$\nabla^2\phi = 0 \qquad [1]$$

with the boundary conditions (at the insulators and planes of symmetry)

$$\frac{\partial\phi}{\partial x} = 0 \quad \text{at } x = 0 \text{ and } x = l \text{ for all } y \qquad [2]$$

$$\frac{\partial\phi}{\partial y} = 0 \quad \text{at } y = b,\ 0 \leqslant x < \frac{l}{2} \qquad [3]$$

Since the anode is unpolarized, the potential in the electrolytic solution is equal to the set potential of the anode ϕ_A, and is uniform along its surface

$$\phi = \phi_A \text{ at } y = b,\ \frac{l}{2} \leqslant x < l \text{ (reversible anode)} \qquad [4]$$

At the cathode surface for a primary current distribution, the cathode remains unpolarized

$$\phi = \phi_C = 0 \text{ at } y = h \text{ for all } x \text{ (reversible cathode)} \qquad [5]$$

Note that the height h of the deposit defined in Eq. 5 varies both as a function of time t and the position x. Initially at time $t = 0$, the

* Electrochemical Society Active Member.
** Electrochemical Society Fellow.
z E-mail: subramanian@tntech.ed

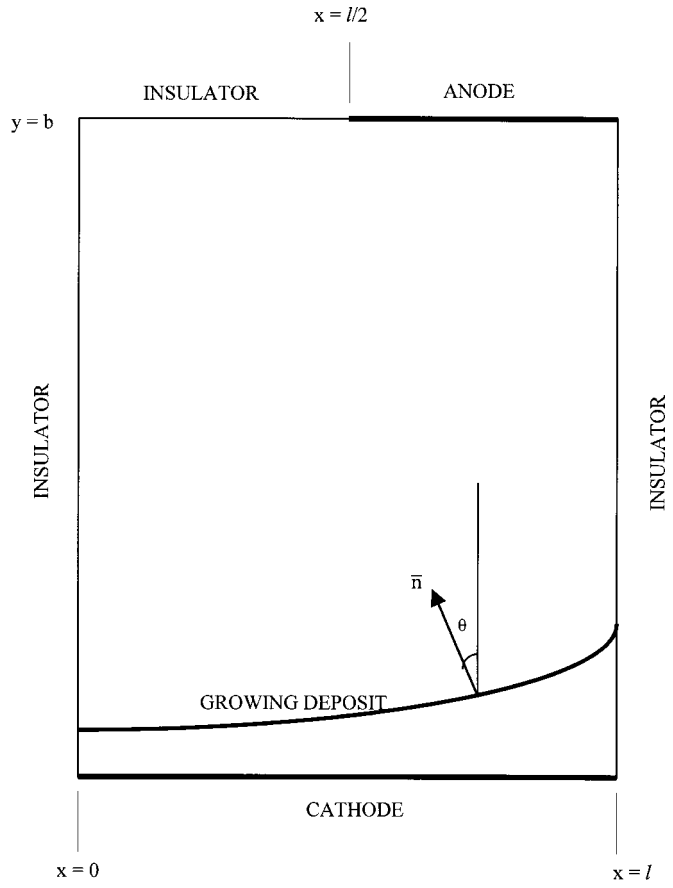

Figure 1. Cell geometry prior to shape change at cathode.

deposit thickness h is zero. Equations 1-5 provide the current and potential distribution within the cell for any particular surface shape. At any instant in time, the local growth of the cathode surface is given by Faraday's law

$$\frac{dh}{dt} = -\frac{M}{n\rho F}\, i = \frac{M\kappa}{n\rho F}\frac{\partial \phi}{\partial y_{y=h}} \qquad [6]$$

This is a moving boundary problem with moving boundary (cathode shape) defined by Eq. 6. The governing equations are made dimensionless using the following variables

$$\Phi = \frac{nF}{RT}\,(\phi - \phi_C);\; X = \frac{x}{l};\; Y = \frac{y}{l};\; A = \frac{b}{l} \qquad [7]$$

$$H = \frac{h}{l} \qquad [8]$$

and

$$\tau = \frac{M\kappa RT}{l^2 n^2 F^2 \rho}\, t \qquad [9]$$

The model equations become

$$A^2\,\frac{\partial^2 \Phi}{\partial X^2} + \frac{\partial^2 \Phi}{\partial Y^2} = 0 \qquad [10]$$

$$\frac{\partial \Phi}{\partial X} = 0 \text{ at } X = 0 \text{ and } X = 1 \text{ for all } Y \qquad [11]$$

$$\frac{\partial \Phi}{\partial Y} = 0 \text{ at } Y = 1,\; 0 \leq X < \frac{1}{2} \qquad [12]$$

$$\Phi = \Phi_A \text{ at } Y = 1,\; \frac{1}{2} \leq X < 1 \text{ (reversible anode)} \qquad [13]$$

$$\Phi = 0 \text{ at } Y = H \text{ for all } X \text{ (reversible cathode)} \qquad [14]$$

$$\frac{dH}{d\tau} = \frac{\partial \Phi}{\partial Y_{\text{at cathode, Y=H}}} \qquad [15]$$

with the initial condition

$$H(\tau = 0) = 0 \qquad [16]$$

Note that no initial conditions are required for $\Phi(X,Y)$. The above dimensionless groups were presented earlier by Alkire *et al.*[7] Equations 10-16 constitute the system to be solved in order to determine the shape evolution of the cathode with time [*i.e.*, $H(\tau)$].

Secondary current distribution.—For secondary current distributions, the reaction rate obeys both Ohm's law and Butler-Volmer kinetics at the cathode surface

$$i = -\kappa\,\frac{\partial \phi}{\partial \bar{n}_{y=h}} = i_0\left[e^{\alpha_A nF/RT\phi} - e^{-\alpha_C nF/RT\phi}\right]_{y=h} \qquad [17]$$

where $\bar{n}$ is the inward normal directed from the cathode surface (Fig. 1). Initially, the normal vector $\bar{n}$ is in the same direction as the y axis, but the direction of $\bar{n}$ changes with time as the deposit grows on the cathode surface. This change of direction of $\bar{n}$ is included in our model as explained below. Equation 17 can be converted to dimensionless form

$$\frac{\partial \Phi}{\partial \bar{n}_{Y=H}} = -I_0\left[e^{\alpha_A \Phi} - e^{-\alpha_C \Phi}\right]_{Y=H} \qquad [18]$$

where I_0 is the dimensionless exchange current density defined by

$$I_0 = \frac{i_0\; l\, nF}{\kappa RT} \qquad [19]$$

In this case, the deposit growth rate in the Y direction is defined by

$$\frac{dH}{d\tau} = \frac{\partial \Phi}{\partial Y_{\text{cathode}}} = \frac{\partial \Phi}{\partial \bar{n}_{\text{cathode}}}\cos\theta \qquad [20]$$

where θ is the angle between the Y axis and the normal vector $\bar{n}$. Note that $\theta = 0$ at $\tau = 0$. θ changes with both τ and X. In this investigation, we restrict the growth of deposit to the Y dimension only.

Equations 10-13, 16, 18, and 20 constitute the system of equations to be solved to determine the evolution of the cathode shape with time $[H(\tau)]$ for a secondary current distribution, given values for A, I_0, Φ_A, α_A, and α_C. Existing methods in the literature require specifying an initial guess for the distribution of the potential for solving Butler-Volmer boundary conditions. Our method does not require any initial guesses for the potential distribution.[5]

Semianalytical Technique

The computational method consists of applying finite difference approximations for the derivatives which are accurate to the order $(\Delta X)^2$ in the X axis and integrating the resulting equations analytically in Y. This method converts the Laplace equation and the boundary conditions at $X = 0$ and $X = 1$ to a system of coupled second order linear ordinary differential equations in Y for the values of the potentials at the interior node points i (Φ_i).[5] The potential along the line $X = 0.5$ has a singularity at $Y = 1$. Consequently, to remove the need to specify a boundary condition for Φ at $X = 0.5$ and $Y = 1$, the potential along the line ($X = 0.5$) is eliminated by equating the backward and forward flux of potentials at $X = 0.5$ for all Y except $Y = 1$.[5] For example, when $N = 13$ interior node

points are used, the seventh interior node point $(N + 1)/2$ corresponds to the line $X = 0.5$. The potential at this line is eliminated by requiring that the current in the X direction be continuous

$$\frac{\partial \Phi}{\partial X}_{X=0.5-} = \frac{\partial \Phi}{\partial X}_{X=0.5+} \quad [21]$$

Equation 21 can be written in finite difference form

$$\frac{1}{2}\frac{3\Phi_{(N+1)/2} - 4\Phi_{(N-1)/2} + \Phi_{(N-3)/2}}{\Delta x} = \frac{1}{2}\frac{-3\Phi_{(N+1)/2} + 4\Phi_{(N+3)/2} - \Phi_{(N+5)/2}}{\Delta x} \quad [22]$$

where $\Delta X = 1/(N + 1)$ and Eq. 22 can be solved for $\Phi_{(N+1)/2}$

$$\Phi_{(N+1)/2} = \frac{2}{3}(\Phi_{(N+3)/2} + \Phi_{(N-1)/2}) - \frac{1}{6}(\Phi_{(N+5)/2} + \Phi_{(N-3)/2}) \quad [23]$$

Note that to include $X = 0.5$ as a node point, N should be chosen as an odd number.

The Laplace equation is discretized in the X axis using finite differences with N interior node points. The potentials at the 0th and $N + 1$th node points are given by the boundary conditions at $X = 0$ and 1, respectively (Eq. 11). The potential at $X = 0.5$ [$(N + 1)/2$th node point] is given by Eq. 23 and is used to remove explicit dependence of the potential at node $(N + 1)/2$ from the system of equations. So when N interior node points are used, the Laplace equation is converted to $N - 1$ linear coupled second order differential equations in Y.[5] These equations are then integrated using the matrix exponential matrix method.[5] For a primary current distribution case, when N interior node points are used, the deposit growth rate is given by $N - 1$ simultaneous first order ordinary differential equations

$$\frac{d\mathrm{H_i}}{d\tau} = \frac{\partial \Phi_i}{\partial Y}_{Y=\mathrm{H_i}} = c_i, \quad i = 1 \ldots N, \quad i \neq (N + 1)/2 \quad [24]$$

where c_i is the potential derivative $(\partial\Phi/\partial Y)$ at the cathode surface at the various interior node points (*i.e.*, $c_i = \partial\Phi_i/\partial Y_{x_i}$ where $X_i = i\Delta X$ for $i = 1 \ldots N$, $i \neq (N + 1)/2$). The boundary conditions at $Y = 1$ are given by

$$f_i(H_i(\tau), \; c_{i,i=1\ldots N, i\neq(N+1)/2}) = 0 \quad i = 1 \ldots N, \quad i \neq (N + 1)/2 \quad [25]$$

The functions f_i values are obtained in the same manner as those given by Eq. 31 and 32 in Ref. 5, however, the f_i values obtained here are too long to be included. (These f_i values are available upon request from the authors.) Thus, the problem is reduced to $2N - 2$ unknowns (H_i and c_i at $i = 1 \ldots N$, $i \neq (N + 1)/2$) whose values are obtained by solving the $N - 1$ simultaneous first order ordinary differential equations (ODEs) given by Eq. 24 and $N - 1$ algebraic equations given by Eq. 25. Equations 24 and 25 constitute the governing equations for predicting the cathode shape changes for primary current distributions.

Equations 24 and 25 developed above for primary current distributions are also valid for secondary current distributions (Eq. 20 and 18). However, in secondary current distributions, the c_i values are given by the Butler-Volmer equation[5]

$$c_i = -I_0[e^{\alpha_A \Phi_i} - e^{-\alpha_C \Phi_i}]_{y=\mathrm{H}} \cos\theta, \quad i = 1 \ldots N, \quad i \neq (N + 1)/2 \quad [26]$$

So for secondary current distribution, the given moving boundary problem is reduced to $N - 1$ simultaneous first order ODEs given by Eq. 24 with $2N - 2$ algebraic equations given by Eq. 25 and 26. Equations 24-26 constitute the governing equations for predicting the shape changes for secondary current distribution. The steps involved in the simulation can be summarized as follows.

1. Laplace equation (Eq. 10) is discretized in the X direction by applying finite differences with N equally spaced interior node points.

2. The boundary values for the potential at $X = 0$ and $X = 1$ are eliminated using the boundary conditions (Eq. 11).

3. The potential along the line $X = 0.5$ [$i = (\mathrm{N} + 1)/2$] is eliminated using Eq. 23.

4. The potential derivatives at $Y = \mathrm{H}$ (at the interior node points) are specified as c_i, where i goes from 1 to N ($i \neq (\mathrm{N} + 1)/2$).

5. The problem is reduced to $2N - 2$ unknowns (H_i and c_i at $i = 1 \ldots N$, $i \neq (N + 1)/2$) whose values are obtained by solving the $N - 1$ simultaneous nonlinear ODEs in time (Eq. 24) coupled with $N - 1$ algebraic equations (Eq. 25) for primary current distributions. For secondary current distributions, the problem is reduced to $3N - 3$ unknowns (H_i, c_i, and Φ_i at $i = 1 \ldots N$, $i \neq (N + 1)/2$) whose values are obtained by solving the $N - 1$ simultaneous nonlinear ODEs in time (Eq. 24) coupled with $2N - 2$ algebraic equations (Eq. 25 and 26). For both primary and secondary current distributions, a symbolic solution is obtained for the potential and current distributions for a given geometry.[5] These symbolic solutions are general and valid for any cathode shape, polarization parameter I_0, aspect ratio A, and size of cathode and anode.[5,14] These symbolic solutions are also valid for any boundary condition on the cathode and anode (for example, see Eq. 44, 47, and 50 in Ref. 5).

6. The functions f_i defined in Eq. 25 depend on the boundary condition at $Y = 1$. For values of $X < 0.5$ [$i < (N + 1)/2$] f_i is given by the insulator boundary condition. For values of $X > 0.5$ [$i > (N + 1)/2$], f_i is given by the boundary condition at the anode surface ($\Phi_i = \Phi_A$).

7. Potential and current distributions are obtained for the given geometry at time $\tau = 0$. These symbolic solutions are valid for both the primary and secondary current distributions. For primary current distributions, the values of A, Φ_A, and N are fixed. This gives a symbolic expression for the functions f_i defined in Eq. 25. The functionality f_i defined in Eq. 25 is a function of deposit thickness at the ith node point, $H_i(\tau)$ and the potential gradients, c_i. The $N - 1$ algebraic equations (Eq. 25) are solved simultaneously to give the current distribution at $Y = H$ (cathode surface) at $\tau = 0$; *i.e.*, unknown constants c_i [$i = 1 \ldots N$, $(i \neq (N + 1)/2]$. Note that at time $\tau = 0$, the thicknesses at all the interior node points [$H_i(\tau)$] are all zero. A time step of $\Delta\tau$ is chosen and Eq. 24 is integrated by using Maple with Euler's explicit forward integration

$$H_i(\tau + \Delta\tau) = H_i(\tau) + c_i\Delta\tau, \quad i = 1 \ldots N, \quad i \neq (N + 1)/2 \quad [27]$$

8. Once the new thicknesses [$H_i(\tau + \Delta\tau)$] at the interior node points are estimated using Eq. 27, the new values of thickness $H_i(\tau + \Delta\tau)$ are substituted in the functions f_i in Eq. 25. These $N - 1$ algebraic equations are again solved for the c_i values to give the current distribution at $Y = H_i$ at $\tau = \tau + 2\Delta\tau$. These new values of c_i, [$i = 1 \ldots N$, $(i \neq (N + 1)/2]$ are then substituted into Eq. 27 to find the new thickness $H_i(\tau + 2\Delta\tau)$.

9. Step 9 is repeated and the shape evolution of cathode surface is obtained.

10. The same procedure used for primary current distributions is followed for the secondary current distributions also. In addition to solving the $N - 1$ algebraic equations for the functionality f_i de-

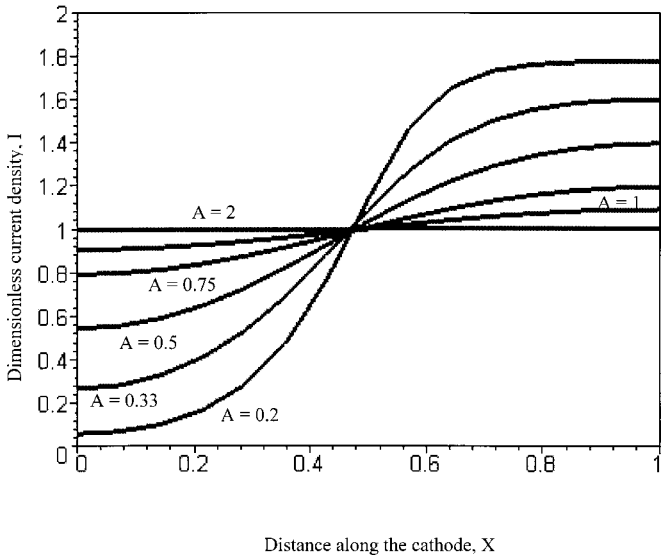

Figure 2. Primary current distribution at $\tau = 0$ – effect of aspect ratio $A = b/l$.

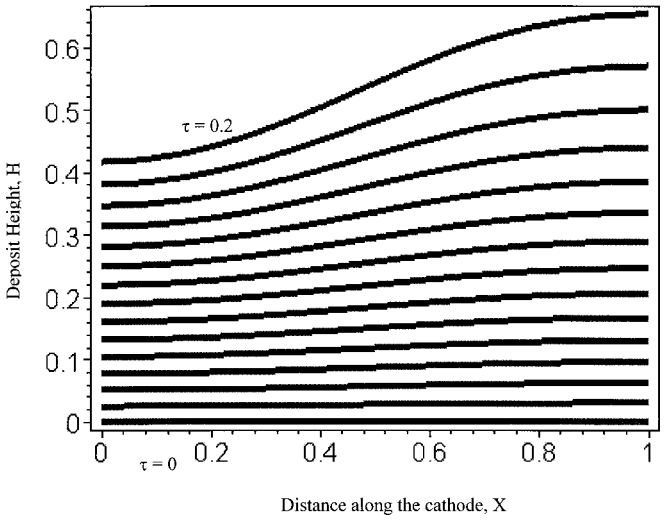

Figure 3. Changing cathode shape governed by primary current distribution ($A = 1$, $\Phi_A = 1$).

fined by Eq. 25 at every time step, $N - 1$ algebraic equations for the Butler-Volmer equation defined by Eq. 26 are solved simultaneously. Also after every time step, the angle between the normal and the Y axis changes (Eq. 20, Fig. 1). This is recalculated after every time step for every node point as

$$\tan[\theta_i(\tau + \Delta\tau)] = \frac{H_i(\tau) - H_{i-1}(\tau)}{h} \qquad [28]$$

This was not necessary for the primary current distributions because the potential at the surface of the cathode ($Y = H$) was known (Eq. 14).

11. If one were to solve for a different configuration or initial sizes of anode or cathode, one has to find Eq. 25 and 26 by using the procedure presented here or in Ref. 5 and repeat the same procedure. There is no need to solve the Laplace equation again. This flexibility is a unique aspect of our technique.

All the figures reported in the next section were obtained by symbolically solving the Laplace equation only once and calculations were redone only in time. All the results reported in this investigation are simulated with $N = 13$ interior node points. Euler's explicit time stepping (Eq. 27) was used in our simulation for the time derivative for convenience. For the examples chosen in this paper, Euler's explicit time stepping was found to be sufficient and the results were verified by decreasing the step size in time. However, it should be noted that depending on the geometry and the problem chosen, Euler's explicit time stepping may not converge and accurate/higher order schemes in time might be needed.

Results and Discussion

The normalized current density at the cathode can be calculated using the average current density as

$$I = \frac{i}{i_{avg}} = \frac{i}{\int_0^1 i dX} \qquad [29]$$

where i is the normal current density at the cathode surface (Eq. 6). The primary current distribution at the cathode at time $\tau = 0$ (immediately before the deposition begins) is plotted in Fig. 2 as a function of the aspect ratio A with $\Phi_A = 1$. All the simulations for primary current distribution were performed with $\Phi_A = 1$ as the primary current distribution is independent of the magnitude of the applied potential, Φ_A.[1] We note that for the geometry chosen, the current density on the cathode surface remains finite, since there is no singular point in the cathode surface. (On the contrary, the current density becomes infinity at the singular point $X = 0.5$; $Y = 1$ in the anode surface). For values of $A > 2$ the current distribution is uniform. As the aspect ratio A decreases, the current distribution becomes highly nonuniform.

During electrodeposition, the deposit grows on the cathode. This means that during deposition, the aspect ratio A decreases and the nonuniformity of current distribution increases. So, the deposit growth becomes more nonuniform as time progresses. This can be quantified by following the deposit growth. The deposit growth is followed in Fig. 3 as a function of time with $A = 1$ and $\Phi_A = 1$ as a function of time τ. Initially at time $\tau = 0$, there is no deposit. As time progresses, the deposit grows over the cathode surface. We observe that the thickness at $X = 0$ is small compared to the thickness at $X = 1$. The uniformity of the deposit obtained can be predicted by finding the ratio of maximum thickness (at $X = 1$) to minimum thickness (at $X = 0$), which can be defined as the shape ratio

$$\text{Shape ratio } (S) = \frac{\text{thickness at } X = 1}{\text{thickness at } X = 0} = \frac{H(1)}{H(0)} \qquad [30]$$

Gill *et al.*[13] used a similar variable for measuring the step coverage during pulse plating of copper. The shape ratio (S) as a function of dimensionless time (τ) is plotted in Fig. 4. Initially at very low values of τ, the shape ratio (S) is 1.2. As the deposition progresses, since the aspect ratio decreases, the current distribution becomes more nonuniform. Hence, the deposit growth becomes increasingly nonuniform. Since primary current distributions depend only on the aspect ratio, the deposit growth nature and shape ratio also depend only on the aspect ratio A. For primary current distribution, we can conclude that for ideal uniform deposit growth, the aspect ratio A should be large. However, by increasing A, the cell resistance is increased and the time taken for deposition increases. So, tradeoffs should be made between deposition cost and uniformity of deposit. One should note that this conclusion is true only for the geometry presented in Fig. 1. The change of cathode shape decreases the aspect ratio with time. This is taken care of in the simulation. Again, as H increases, the aspect ratio decreases, and this is included in the simulation.

For secondary current distributions both the cathode and anode transfer coefficients (α_A and α_B) in Eq. 18 are taken to be 0.5. Current distribution along the cathode at time $\tau = 0$ is plotted in

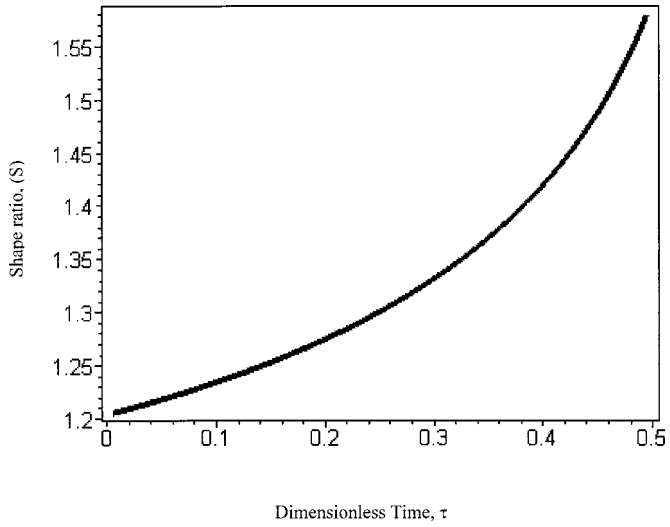

Figure 4. Shape ratio for primary current distribution ($A = 1$, $\Phi_A = 1$).

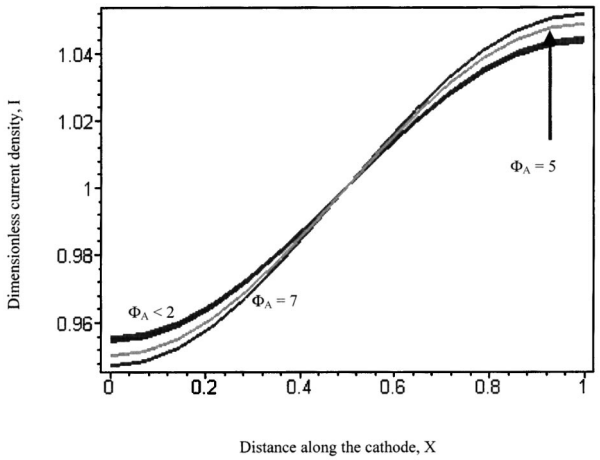

Figure 6. Secondary current distribution at $\tau = 0$ – effect of applied potential Φ_A ($I_0 = 1$, $A = 1$).

Fig. 5 for various values of aspect ratio A at $\tau = 0$ for a set value of parameters $I_0 = 1$ and $\Phi_A = 1$. For values of $A > 2$, the distribution is uniform. As the aspect ratio decreases, the nonuniformity increases. For values of $A < 0.5$, the distribution becomes highly nonuniform.

Secondary current distributions become more nonuniform as the applied potential Φ_A is increased as shown in Fig. 6 for time $\tau = 0$. For this simulation the parameters are taken to be $A = 1$ and $I_0 = 1$. Unlike primary current distributions, secondary distributions are affected by the applied potential Φ_A. For low values of applied potential Φ_A, the distribution is uniform. As the applied potential increases, the distribution becomes more nonuniform.

Secondary current distribution at time $\tau = 0$ across the cathode surface is plotted in Fig. 7 for different values of dimensionless exchange current (polarization parameter I_0) for a set value of parameters $A = 1$ and $\Phi_A = 1$. Note that only the initial aspect ratio is set to be $A = 1$. As the exchange current I_0 increases, the distribution becomes more nonuniform and approaches primary distribution. We observe by comparing Fig. 6 and 7 that I_0 has more effect on the distribution than the applied potential Φ_A.

The deposit growth is followed in Fig. 8 as a function of time for a set value of parameters $A = 1$, $I_0 = 1$, and $\Phi_A = 1$. We note that deposit growth is proportional to the current density and the orientation ($\cos\theta$) according to Eq. 20. We observe that thickness is maximum at $X = 1$ where the current density is the maximum and minimum at $X = 0$ where the current density is minimum as expected.

The shape of the electrode for various values of exchange current I_0 is plotted in Fig. 9 for the same amount of time (τ) passed ($\tau = 0.25$). The parameters are taken to be $A = 1$ and $\Phi_A = 1$. As I_0 increases, the current distribution becomes more nonuniform (Fig. 7). So we observe that as I_0 increases the deposit becomes more nonuniform and we get higher thickness. However this conclusion can be misleading because $A = 1$ corresponds to a uniform current distribution (Fig. 5). If we decrease A to 0.33 we observe different results. The simulated cathode shapes for two different values of exchange current I_0 are plotted in Fig. 10 for the same amount of time passed ($\tau = 0.25$). Here, $I_0 = 10$ corresponds to highly nonlinear distribution and the deposit growth is less for $X < 0.2$ compared to $I_0 = 1$. But for values of $X > 0.2$, we observe thicker

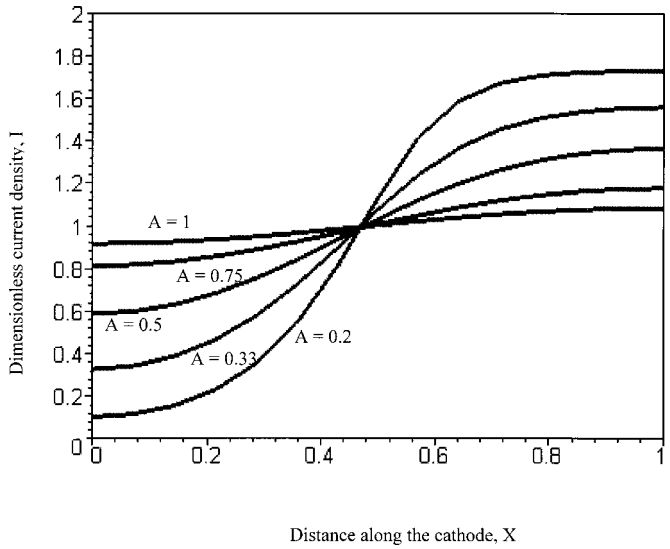

Figure 5. Secondary current distribution at $\tau = 0$ – effect of aspect ratio A ($I_0 = 1$, $\Phi_A = 1$).

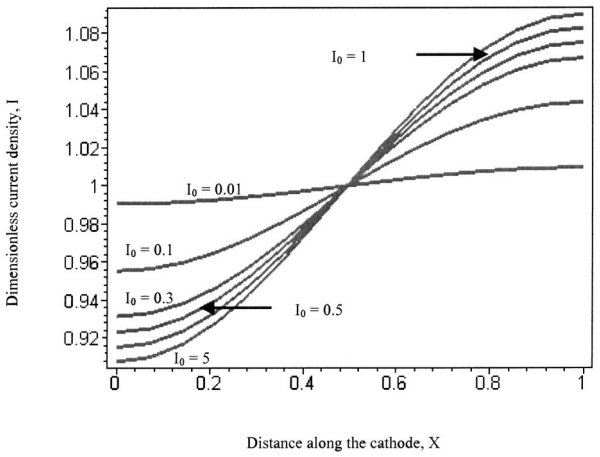

Figure 7. Secondary current distribution at $\tau = 0$ – effect of exchange current I_0 ($A = 1$, $\Phi_A = 1$).

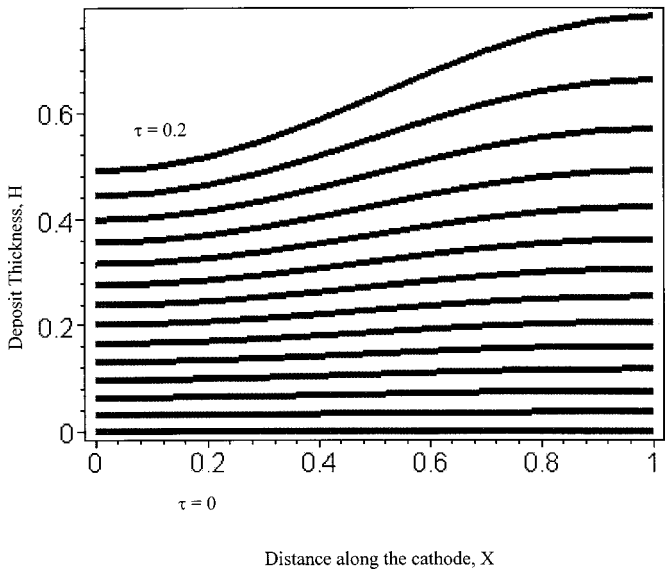

Figure 8. Changing cathode shape governed by secondary current distribution-semianalytical method ($A = 1$, $\Phi_A = 1$, $I_0 = 1$).

deposit for $X > 0.2$ compared to $I_0 = 1$. So there can be an optimum value for I_0 to ensure minimum thickness and maximum uniformity.

The shape ratio (S) is plotted in Fig. 11 as a function of time for different values of I_0 for set values of the parameters, $A = 1$ and $\Phi_A = 1$. Shape ratio increases as a function of time τ. We observe that shape ratio is less for secondary current distribution compared to the primary distribution (Fig. 4). As the exchange current increases, the shape ratio becomes more nonuniform. For both primary and secondary current distributions, we observe that the shape ratio increases with deposition (time). This conclusion is true for only the geometry considered.

The shape ratio (S) at a particular dimensionless time ($\tau = 0.1$) is plotted in Fig. 12 as a function of I_0 for different values of aspect ratios, A, for a fixed value of parameter $\Phi_A = 1$. Shape ratio increases exponentially as a function of time I_0 and then saturates. As the aspect ratio decreases, the current distribution becomes nonuniform and hence, shape ratio becomes more nonuniform. For

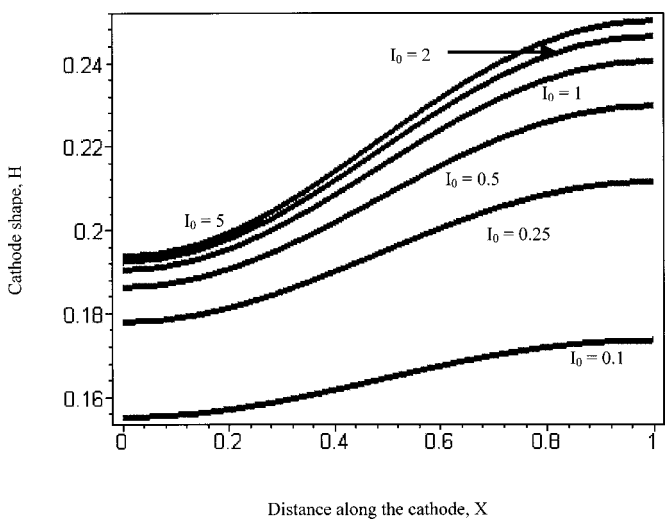

Figure 9. Dependence of changing cathode shape ($\tau = 0.25$) on the exchange current I_0 ($A = 1$, $\Phi_A = 1$).

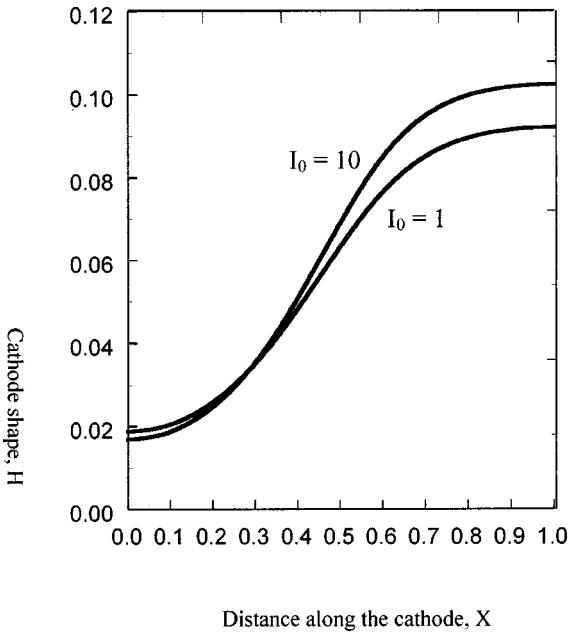

Figure 10. Dependence of changing cathode shape ($\tau = 0.25$) on the exchange current I_0 for smaller aspect ratios ($A = 0.33$, $\Phi_A = 1$).

the geometry chosen, the shape ratio approaches one for high values of aspect ratios because for high aspect ratios, the current distribution is uniform (see Fig. 5).

Shape ratio for a different geometry (anode and cathode are switched in size, Fig. 1) used by Alkire *et al.*,[7] is plotted in Fig. 13. For this case, we observe that shape ratio initially increases marginally and then decreases with time. This happens because of infinite current density at $X = 0.5$. The singularity at $X = 0.5$ is handled by equating the potential derivatives at $X = 0.5$ as described in Ref. 5. So $\cos(\theta)$ in Eq. 20 decreases drastically as we go from $X = 0$ to 0.5. This makes the current distribution uniform as the time progresses as reported in the literature.[7]

Conclusions

The semianalytical method presented earlier[5] is extended to predict shape changes during electrodeposition. The new technique pro-

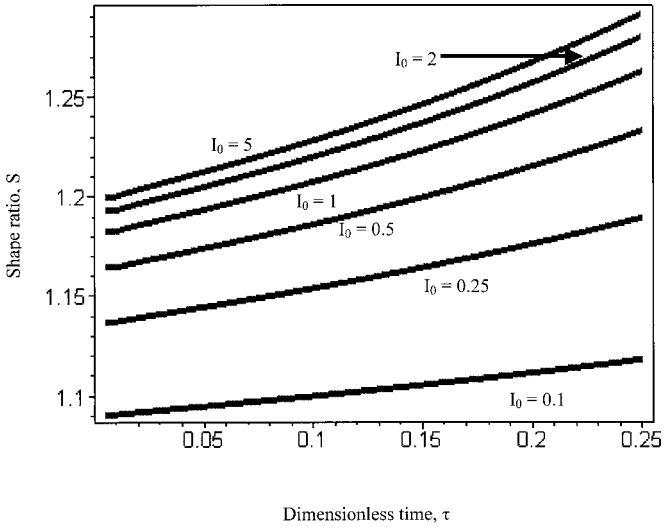

Figure 11. Shape ratio for secondary current distribution − effect of exchange current I_0 ($A = 1$, $\Phi_A = 1$).

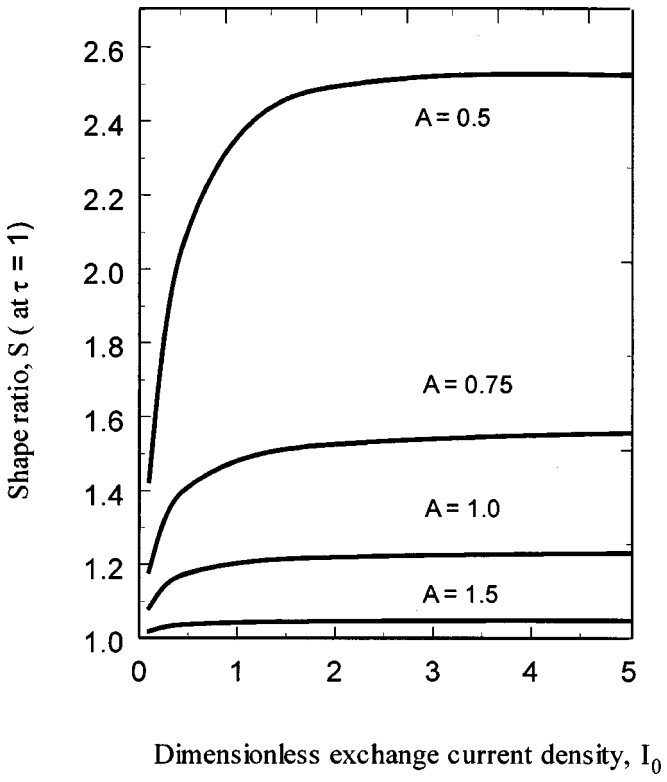

Figure 12. Shape ratio for secondary current distribution − effect of exchange current I_0 and aspect ratio, A ($\Phi_A = 1$).

vides a general symbolic solution for the Laplace equation, which is valid for any boundary conditions on the cathode and anode. The generality of the solution obtained is exploited to predict the shape changes for both primary and secondary current distributions. The shape ratio is found to increase with the deposition for the geometry chosen for both primary and secondary current distributions. This is true because aspect ratio has more impact on the distribution than the kinetics and the applied potential.

Mass transfer models for metal deposition also obey Laplace's equation in two dimension with a changing cathode shape.[11-13,15] The technique developed in this paper should find direct use in these mass transfer models. Future work involves predicting shape changes in two and three dimensions. The extension of the semianalytical technique to three dimensions is straightforward, but the math involved in obtaining a semianalytical solution for 3-D problems is complicated. For example, for Laplace equation in three dimensions, one can apply finite differences in x and z directions and obtain semianalytical solutions in y easily.[16] However, this will help us predict shape changes in the y direction only. If one has to predict the shape changes in both x and y directions, one has to apply finite differences in z only and integrate analytically in both x and y. This integration is not straightforward and we are currently working on integrating matrix equations in two dimensions (x and y). This work will be communicated later. In addition, finite difference expressions of higher order of accuracy can be used to increase the efficiency of the computation.[5] Maple programs used for simulating the shape changes are available upon request from the authors.

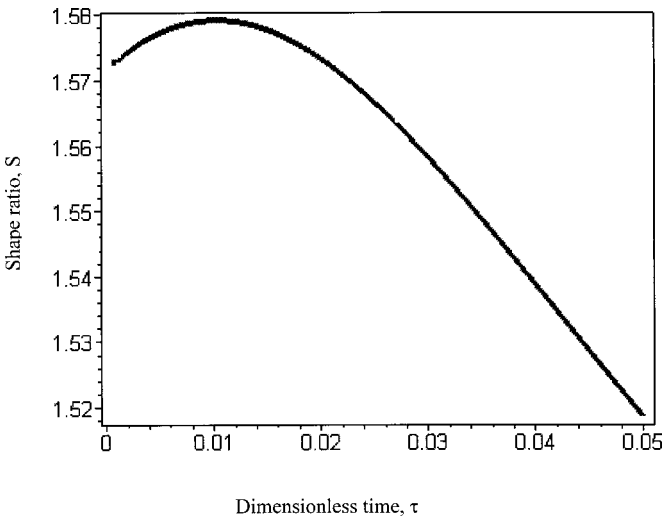

Figure 13. Shape ratio for a different geometry ($A = 1$, $\Phi_A = 1$).

Acknowledgments

The authors are grateful for the financial support of the project by the National Reconnaissance Office (NRO) under contract no. NRO 000-01-C-4368.

The University of South Carolina assisted in meeting the publication costs of this article.

List of Symbols

A	aspect ratio at $\tau = 0$, b/l
b	height of the cell, cm
c_i	dimensionless unknown constants
F	Faraday's constant, 96487 C/g equiv
h	thickness of the deposit, cm
H	dimensionless thickness of the deposit
H_i	dimensionless thickness of the deposit at the node point i
i	current density, A cm^{-2}
i_{avg}	average current density along the cathode, A cm^{-2}
I	dimensionless current density
I_0	dimensionless exchange current density
l	length of the cell, cm
M	molecular weight, g/mol
n	number of electrons transferred in the electrochemical reaction
$\overline{\mathbf{n}}$	inward unit normal to the surface of the cathode (see Fig. 1)
N	total number of interior node points
R	gas constant, 8.3143 J/g mol-deg
S	shape ratio
t	time, s
X	dimensionless spatial coordinate, x/l
ΔX	$1/(N + 1)$
Y	dimensionless spatial coordinate, y/l

Greek

α_A	anodic transfer coefficient
α_C	cathodic transfer coefficient
∇	gradient, cm^{-1}
κ	conductivity, Ω^{-1} cm^{-1}
ϕ	potential, V
ϕ_A	applied anode potential, V
ϕ_C	applied cathode potential, V
Φ	dimensionless potential
Φ_A	dimensionless applied potential
θ	angle between the unit normal to the cathode surface and Y-axis
ρ	density of the deposit, g/cm^3
$\Delta\tau$	dimensionless increment in time

References

1. J. S. Newman, *Electrochemical Systems*, 2nd ed., Chap. 18, Prentice Hall, Englewood Cliffs, NJ (1991).
2. A. C. West and J. S. Newman, in *Modern Aspects of Electrochemistry*, Vol. 23, B. E. Conway, J. O'M. Bockris, and Ralph E. White, Editors, p. 113, Plenum Press, New York (1992).
3. G. Prentice, *Electrochemical Engineering Principles*, p. 195, Prentice Hall, Englewood Cliffs, NJ (1986).
4. J. S. Newman, in *Electroanalytical Chemistry*, Vol. 6, Allen J. Bard, Editor, p. 187, Marcel Dekker, Inc., New York (1973).
5. V. R. Subramanian and R. E. White, *J. Electrochem. Soc.*, **147**, 1636 (2000).
6. R. Varma and J. R. Selman, *Characterization of Electrodes and Electrochemical Processes*, Chap. 13, John Wiley & Sons, Inc., New York (1991).
7. R. Alkire, T. Bergh, and R. L. Sani, *J. Electrochem. Soc.*, **125**, 1981 (1978).
8. G. A. Prentice and C. W. Tobias, *J. Electrochem. Soc.*, **129**, 78 (1982).
9. G. A. Prentice and C. W. Tobias, *AIChE J.*, **129**, 486 (1982).

10. A. C. West, C. Madore, M. Matlosz, and D. Landolt, *J. Electrochem. Soc.*, **139**, 499 (1992).
11. M. Georgiadou, D. Veyret, R. L. Sani, and R. C. Alkire, *J. Electrochem. Soc.*, **148**, C54 (2001).
12. A. C. West, C. C. Cheng, and B. C. Baker, *J. Electrochem. Soc.*, **145**, 3070 (1998).
13. W. N. Gill, D. J. Duquette, and D. Varadarajan, *J. Electrochem. Soc.*, **148**, C289 (2001).
14. P. S. Fedkiw, *J. Electrochem. Soc.*, **128**, 831 (1981).
15. C. Madore, O. Piotrowski, and D. Landolt, *J. Electrochem. Soc.*, **146**, 2526 (1999).
16. V. R. Subramanian and R. E. White, Unpublished results.